Interphase Evolution in Polymer Films by Confocal Raman Microspectroscopy

J. PABLO TOMBA,* JOSÉ M. CARELLA, and JOSÉ M. PASTOR

Institute of Materials Science and Technology (INTEMA), National Research Council (CONICET), University of Mar del Plata, Juan B. Justo 4302, (7600) Mar del Plata, Argentina (J.P.T, J.M.C.); and Department of Physics of Condensed Matter, University of Valladolid, Paseo del Cauce s/n, (47011) Valladolid, España (J.M.P.)

Liquid-glassy polymer diffusion is an important topic in polymer physics, with several mechanistic aspects that still remain unclear. Here we describe the use of confocal Raman microspectroscopy (CRM) to study directly several features of interphase evolution in a system of this type. The interphase studied was generated by contact between liquid polystyrene (PS) and glassy polyphenylene oxide (PPO). Interphase evolution on thin films made from these polymers was followed by depth profiling in combination with immersion optics. We also applied regularized deconvolution to improve the spatial resolution of the measurements. With the help of these techniques, we examined interphase PPO concentration profiles and kinetics of interphase evolution in the range 120–180 °C, well below the glass transition temperature of the PPO-based films (185 °C). Overall, the experiment captures the most important features needed to discern the mechanistic factors that control this process. In this sense, confocal Raman microspectroscopy emerges as one of the best experimental techniques for the study of diffusion kinetics in this type of system.

Index Headings: **Polymer interphases; Confocal Raman microspectroscopy; CRM; Depth profiling; Spatial deconvolution.**

INTRODUCTION

Polymeric interphases play a central role in many technological applications. In polymer blends and alloys, interactions at the original interface affect the morphology of the system in the melt and the transmission of stresses in the solid state. In various processes related to polymer welding, the diffusion of polymer molecules across the interphase is the mechanism of growth in adhesive strength. A precise control of the interphase generated by contact between a glassy polymer and low molecular weight liquids is crucial in microlithography and drug delivery systems, as well as in many polymer-based products such as latex and polymer blends with hard and soft components, among others.

In parallel to their importance in industrial applications, polymeric interphases have stimulated a vast body of fundamental research. The principles that govern interphase evolution in entangled polymer melts are well established and can be described using the theory of liquid dynamics in combination with the reptation model developed by de Gennes.[1,2] On the contrary, the mechanisms of interphase evolution in systems involving one of the polymers in the glassy state still offer many aspects not completely understood. For example, the penetration and diffusion of small-size molecules in glassy polymers gives rise to a remarkable non-Fickean diffusion mechanism called Case-II.[3] The central feature of Case-II is a process of interphase evolution controlled by the mechanical relaxation of the glassy polymer, in response to the osmotic swelling stress associated with the small molecules' penetration. The mechanism is characterized by a sharp front in the small molecule concentration profile, which propagates through the polymer film with distinctive (linear) diffusion kinetics. Whether these unique features observed in the case of small molecules can be extended to the case of larger molecules, i.e., oligomers and polymers with moderate molecular weight above their glass transition temperature (T_g), is a topic that remains in debate, as shown by much recent work published on this subject.[4–7]

Among the battery of techniques applied to study polymer interphases, direct methods, capable of measuring point-by-point chemical composition along a given direction, have gained prominence. They provide a straightforward description of the interphase that can be analyzed and interpreted without resorting to previously assumed models. Over the last two decades, direct methods such as forward recoil spectroscopy (FRES),[8] Rutherford backscattering spectrometry (RBS),[9] and nuclear reaction analysis (NRA)[10] have been extensively employed to study kinetics of polymer interphases, helping to gain most of our understanding on the factors that control their evolution.

Confocal Raman microspectroscopy (CRM) also falls into the category of direct methods. Like no other, CRM offers a unique combination of moderate spatial resolution and high sensitivity to C–C and C=C structures that commonly constitute the backbone of polymeric materials. Although FRES, RBS, and NRA provide information on a finer scale than CRM, they require extensive labeling of the polymer chain with heavy atoms (usually deuterium), which demands specialized synthesis and may change the thermodynamic interactions in the system.[11] Requiring minimum sample preparation, CRM provides enough spatial resolution to measure diffusion coefficients in the range 10^{-7}–10^{-13} cm^2/s, which makes the technique especially suitable for the study of diffusion kinetics in a wide range of systems involving oligomers and moderate molecular weight polymers. Confocal fluorescence microspectroscopy operates under similar principles as CRM, but has the disadvantage that fluorescence intensity is not simply related to chemical composition.[12] Compared with CRM, scanning infrared microscopy (SIRM) offers spatial resolution on a coarser scale.[13]

Despite its potential to measure interphase composition directly, only a few groups have explored the use of CRM to follow diffusion kinetics in polymer systems.[14–16] In all these studies, the use of depth profiling with standard metallurgical objectives to study different aspects of the interphase has been a common feature. It has been well documented that the use of "dry" metallurgical objectives, commonly attached to most of the commercial microspectrometers, severely deteriorates the depth resolution of the instrument due to laser beam refraction

Received 11 November 2005; accepted 21 December 2005.
* Author to whom correspondence should be sent. E-mail: jptomba@fi.mdp.edu.ar.

0003-7028/06/6002-0115$2.00/0

at the air–sample interface. This problem, first quantified by Everall,[17,18] has received subsequent attention by many other authors.[19–21] Essentially, refraction produces a geometric shifting of the focal point at higher depths into the sample and a progressive increase of the span of depths effectively illuminated by the laser beam, well beyond the nominal diffraction limit. As a result, sharp interphases appear significantly broadened and the depth scale appears artificially distorted, complicating data interpretation. These problems can be avoided with the use of immersion objectives. In this case, a fluid that matches the refractive index of the sample fills the space between the objective and the sample, minimizing refraction of the laser beam and thus improving depth resolution.

In this work, we report on the first studies of interphase evolution using depth profiling in combination with immersion optics by CRM. We focus on the study of a relevant liquid-glassy polymer interphase, in this case between oligomeric polystyrene- and polyphenylene oxide-based films. The experimental setup used, originally conceived as a bench-test for diffusion studies in this type of system, is described. We also consider the application of regularized deconvolution to improve the spatial resolution of the measurements. Equipped with these techniques, CRM gains in flexibility and accuracy, emerging as possibly the most suitable tool for the study of this type of polymeric interphase.

EXPERIMENTAL

Polymer films were made from poly-phenylene oxide (PPO) and polystyrene (PS). The PPO sample was obtained from Aldrich ($M_w = 31\,000$ g/mol, $M_w/M_n = 2.0$, $T_g = 212$ °C). The PS sample ($M_w = 740.0$ g/mol, $M_w/M_n = 1.05$, $T_g = -5$ °C) was purchased from Polymer Source (Dorval, Canada). The oil used as immersion fluid ($n = 1.5$, from Merck, catalogue number B446082) was supplied by the microscope objective manufacturer (Olympus). Polymer blends for films were prepared by freeze drying, using benzene as a common solvent. The high T_g blend (glassy film, $T_g = 185$ °C) contains 95 wt. % PPO. The low T_g blend (liquid film, $T_g = 25$ °C) contains 70 wt. % PS.

Cylindrical two-layer specimens (6.5 mm in diameter) were prepared by a sequential two-step process under vacuum inside a specially designed mold with controlled temperature. First, a thin film of the high T_g blend was molded at a temperature above its T_g and the film thickness was directly measured at room temperature with a micrometer. Next, an aluminum guard ring was placed and secured on top of the high T_g film. The guard ring is used to allow liquid diffusion in one direction only. Last, a thick layer of the low T_g blend was vacuum molded on top of the high T_g blend layer in the cavity formed by the aluminum guard ring. The molding temperature for this stage was much lower than that of the high T_g blend to prevent any appreciable diffusion process from taking place. Finally, the total specimen thickness was measured at room temperature with a micrometer.

The composite films were annealed in a temperature-controlled oven (±0.5 °C), continuously flushed with dry nitrogen to avoid polymer oxidation. The samples were periodically removed from the oven and allowed to quickly cool back to room temperature, which virtually stops interphase evolution, before Raman measurements were performed.

Raman spectra were recorded at room temperature, on a Raman microspectrometer DILOR LabRam Confocal, equipped with a 16 mW HeNe laser beam (632.8 nm wavelength). A slit opening of 500 μm and a holographic grating of 1800 lines/mm were used, rendering a spectral resolution of 5 cm^{-1}. We used an immersion Olympus 100× objective (NA =1.3, 210 μm working distance) in combination with a pinhole opening of 800 μm (the maximum aperture is 1000 μm). Some measurements were also carried out with a dry Olympus 100× objective (NA = 0.9, 210 μm working distance). Physical sectioning in some of the specimens was performed at room temperature with a microtome (Leica RM2055). For optical sectioning by depth profiling, the samples were mounted on a microscope stage with vertical displacement (z-axis) controlled manually with the micrometric screw of the microscope. A drop of oil was placed between the glassy layer and the microscope objective just before confocal Raman profiling were carried out. The oil was exhaustively removed with tissue paper before sample annealing. The nominal depth resolution under these instrumental conditions was measured by scanning in the z direction a polished and flat silicon wafer immersed in the oil. Figure 1 shows the intensity profile obtained by integrating the Si line at 520 cm^{-1} as a function of depth. The full-width at half-maximum (FWHM) of this curve, often referred to in the literature as depth resolution, was about 6 μm.

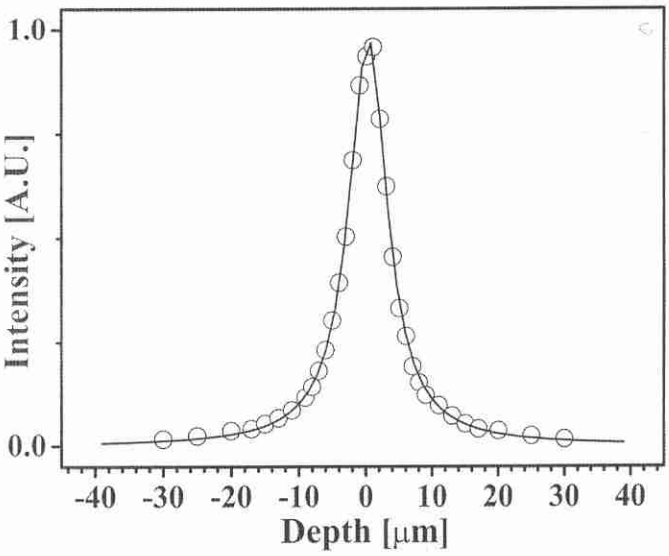

FIG. 1. Step response of a silicon wafer, scanned in the z direction. The open circles correspond to experimental values. The continuous line corresponds to the Lorentzian function used to fit the data.

Composite films were mounted on the microscope stage, supported in a specially designed sample holder, which allows, with the help of the x-y motorized microscope stage, the laser beam to always be focused within ±10 μm of the same sample spot. Concentration depth profiles at the glassy-liquid polymer interphase were measured by taking Raman spectra from different depths while moving the stage vertically (z) in steps of 2–5 μm. The acquisition time for each spectrum was 10 s, and 5 spectra were accumulated for each data point. The acquired Raman spectra were translated to local PS or PPO concentrations (weight fraction) with the linear decomposition method.[22] The method computes the individual contributions of pure components to the global blend spectrum and calculates

the blend composition from the relative contributions and a calibration curve.

RESULTS AND DISCUSSION

Spectral Properties of Polymer Films. Raman spectra of the pure polymers, of their blends, and of the oil used in the immersion objective are shown in Figs. 2A and 2B for Raman shifts recorded in the range 500–1400 cm^{-1}. As shown in Fig. 2A, the individual polymers show characteristic profiles of Raman bands in the spectral range analyzed, making the polymer pair suitable for quantitative analysis.[22] The Raman spectrum of PS presents two intense bands at 1000 and 1030 cm^{-1} corresponding to mono-substituted benzene ring modes.[23] The PPO Raman spectrum shows seven sharp bands, with the two most intense at 1300 cm^{-1} (tentatively assigned to $-CH_3$ bending[23]) and 550 cm^{-1}. Figure 2B shows the Raman spectra of the blends used to make the films. We remind the reader that the individual films are not made out of pure polymers but from PS/PPO blends. We blended the polymers to facilitate the processing and manipulation of the films, taking advantage of the fact that PS/PPO is a quite unique polymer pair that shows full miscibility in the whole range of compositions.[24] While the glassy film contains mostly PPO (95 wt. % PPO, $T_g = 185$ °C), the softer or "liquid" film is far richer in PS (70 wt. % PS, $T_g = 25$ °C). From Fig. 2B, we observe that the composite blend spectra are simply the addition of those of the pure components and that they do not reveal significant shifting and/or broadening of Raman peaks due to PS–PPO interactions. The triplet centered at 1000 cm^{-1} is very sensitive to changes in PS/PPO composition even though the method used to calculate this parameter employs the whole spectral range.[22]

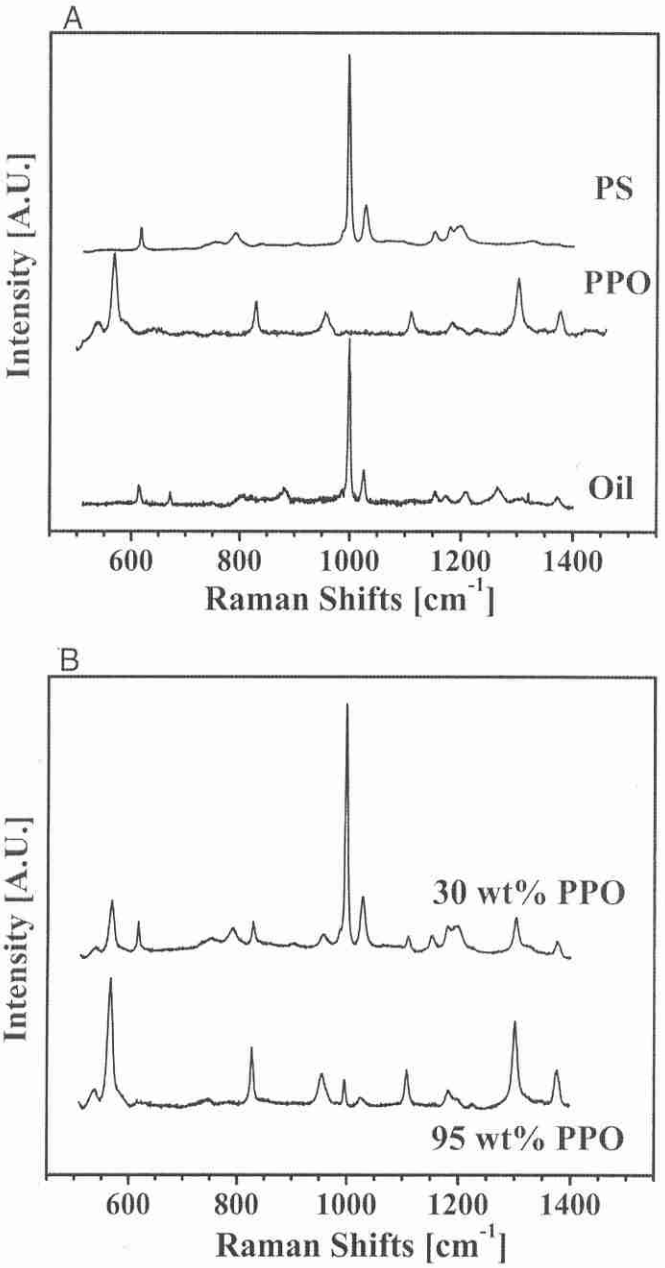

FIG. 2. Raman spectra of individual components: (**A**) pure components; (**B**) polymer blends employed in the films.

Focusing Methods in Confocal Raman Microspectroscopy. Confocal Raman microspectroscopy offers different focusing strategies, summarized in Fig. 3, to study the sample region of interest. The system exemplified corresponds to our liquid-glassy polymer films in contact through a planar interface in such a way that interphase evolution occurs in one direction only. The scheme illustrates the position of the original interface relative to the optical axis of the microscope (solid arrows) and the scanning direction (dotted arrows).

In surface profiling (SP), the scanning direction is normal to the microscope optical axis. This focusing mode yields, in theory, the best spatial resolution (lateral, 1–2 μm), but requires physical sectioning of the sample to expose the interphase to the laser beam. With depth profiling (DP), one can perform optical sectioning of the sample, which would allow, for instance, continuous monitoring of the interphase in a non-destructive way. Depth profiling can be performed either through the glassy layer (DPg) or through the viscous liquid layer (DPl). The disadvantage of this focusing mode is that the depth resolution (axial) is very sensitive to the optics used to focus/collect light, as discussed earlier. With "dry" metallurgical objectives, refraction of the laser beam at the air–sample interface increases the nominal values of depth resolution (2–4 μm, valid at the sample surface) to values on the order of tens of micrometers well inside the sample.[17] The use of immersion objectives with a fluid that matches the sample refractive index

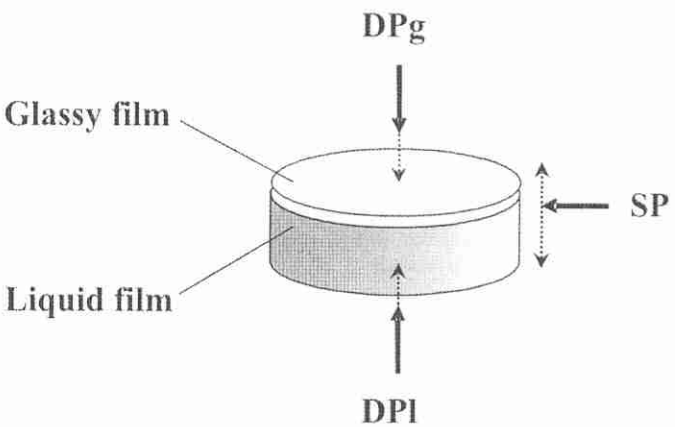

FIG. 3. Scheme of the different focusing strategies in CRM. (**SP**) Surface profiling; (**DPg**) depth profiling through the glassy layer; and (**DPl**) depth profiling through the liquid layer. The dotted arrows represent the scanning direction; the solid arrows represent the optical axis of the microscope.

minimizes refraction aberrations, keeping depth resolution close to the diffraction-limited nominal values. A second benefit gained by working with matched refractive indices when compared with dry optics is that the collection efficiency of Raman photons is increased, as light refraction reduces the solid angle of collection through the pinhole and consequently the number of Raman photons that reach the detector.[19]

Figure 4 compares the confocal Raman response to a very sharp polymer–polymer interface, measured with the focusing approaches outlined before. The plot shows concentration profiles (PPO wt. % versus spatial coordinate) obtained by scanning a 190 μm thick PPO-rich glassy film in contact with a much thicker PS-rich film in a configuration similar to that shown in Fig. 3. The zero in the spatial coordinate scale corresponds to the outer surface of the PPO-rich layer. In these experiments, the original low molecular weight PS was replaced by another polymer with higher molecular weight and higher T_g (M_w = 100 000 g/mol, T_g = 100 °C) to facilitate sample microtoming at room temperature.

The PPO concentration profile obtained by surface profiling (open circles) was measured by lateral mapping of a cross-section obtained by physical sectioning of the two-layer film. The transition between layers appears as a very sharp interface, extended over a range of less than 3 μm, in a position that agrees exactly with the nominal thickness of the glassy layer (190 μm). The approach of depth profiling through the glassy layer is exemplified using dry and oil-immersed objectives. In these cases, the spatial coordinate corresponds to the nominal focusing depth as determined from the micrometric screw of the microscope. With a dry objective (solid squares), the interface appears artificially blurred and extended over a 50 μm region. The apparent thickness of the glassy layer is about 130 μm, much less than the real value. The distortion arises from the above-explained refraction aberrations, which act to compress the z-scale and progressively extend the span of depths where Raman scattering is collected. Following Everall's work,[17] the artificial compression of the depth scale is roughly by a factor of n the refractive index of the polymer medium. In our case, the observed compression factor (190 μm/130 μm = 1.46) lies very well between the refractive indices for pure PPO and PS (1.43 and 1.57, respectively[25]). Even though the artificial compression of the depth scale can be corrected by using simple models for ray-tracing,[16,17] the effect of interfacial broadening can only be corrected by spatial deconvolution. The use of immersion optics and a coupling fluid with a refractive index (1.5) similar to that of the polymers effectively minimizes refraction aberrations (solid triangles). In this case, the interface position agrees with the nominal thickness of the glassy layer and the interfacial blurring is substantially diminished, although the broadening is somewhat larger than that observed with surface profiling.

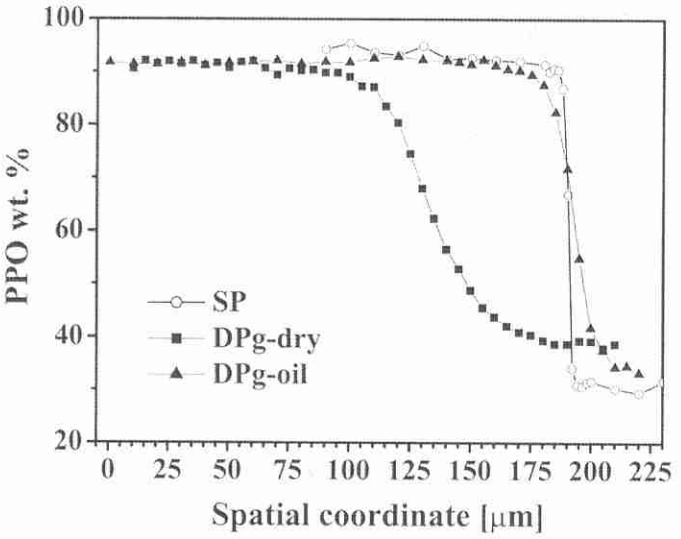

FIG. 4. Raman responses to a sharp polymer–polymer interface, measured by optical sectioning (depth profiling) with dry (DPg-dry) and wet (DPg-oil) objectives, in comparison with physical sectioning and surface profiling (SP). The interface is located at 190 μm.

Design of the Experimental Setup. Although surface profiling resolves details of the interphase with the best spatial resolution, the method requires physical sectioning, a technique particularly difficult to implement in our system as one of the components of the polymer pair is a low molecular weight viscous liquid layer. The requirement of continuous monitoring of the interphase kinetics with moderate spatial resolution in a single sample can only be satisfied by depth profiling in combination with immersion optics, the approach chosen here. However, the use of oil in the optical path of the laser beam and in direct contact with the polymer presents new challenges as it may produce spectral overlapping and/or chemical/physical interaction with the sample.

We discarded the use of oil on the PS-rich film because it is soft and sticky at room temperature and, due to its low molecular weight, it is extremely sensitive to organic penetrants. On the other hand, preliminary tests showed that the highly rigid PPO-rich films are neither affected nor penetrated by the oil used. The surface of the high T_g film remained intact after several hours of exposure to the oil at room temperature, as examined under an optical microscope, and the penetration profile of the oil in the film did not change over time, as measured by CRM. Even though this is not the case here, a wise strategy to avoid oil–polymer interaction is the use of a two-oil configuration with a thin glass as a separating element between the oils.[26] One may use, for example, different oils suitably chosen to be in contact either with the sample or with the objective.

In our case, the oil was applied on the high T_g film, the DPg approach shown in Fig. 2, and the glassy-liquid polymer interphase was profiled through this layer, starting from the oil–high T_g polymer film interface. The initial thickness of the glassy layer (about 190 μm) was just below the working distance of the objective (210 μm) and allows clear observation of the original position of the glassy-liquid polymer interface and, at the same time, a wide span of depths to observe the interphase evolution inside the high T_g film. As we will explain later, the more valuable information on the factors that control interphase evolution in this system originates over this region. Figure 2A shows that the problem of fluid–polymer spectral overlapping is to some extent important between PS and the immersion oil used here. However, because these components are separated by the PPO-rich glassy layer, they do not appear overlapped in the Raman spectra, simplifying the data treatment. Again, the two-oil configuration is a good alternative to avoid the problem that might arise from spectral overlapping.[26]

Interphase Evolution in Glassy-Liquid Polymer Films. Bilayer polymer specimens, such as those shown in Fig. 3, were annealed in the range 120–180 °C for different periods of

time. In this range of temperatures, the PPO-rich film (190 μm thick) remains in the glassy state during the whole process, while the PS-rich layer (1000 μm thick) behaves like a viscous liquid. The PS used for these specimens is the low molecular weight sample described in the Experimental section. To follow interphase evolution we used depth profiling through the glassy layer (DPg in Fig. 3) in combination with immersion optics. Typical interphase profiles, in the form of PPO wt. % versus depth, are shown in Figs. 5A and 5B. The profiles correspond to samples annealed at 160 and 180 °C for the times indicated in the plot.

The plots in Fig. 5 nicely capture the evolution of the glassy-liquid polymer interphase in the composite specimens, revealing important details about the nature of the diffusion process. The glassy layer, initially about 190 μm thick, is progressively thinned by the advance of the liquid PS. The interphase concentration profiles are markedly asymmetric, with the liquid PS advancing as a relatively sharp front between the glassy and liquid layers, followed by a region with much lower slopes at larger focusing depths. The experimental setup allows the direct quantification of two variables, particularly relevant from a mechanistic perspective: the time and the temperature dependence of the liquid front penetration depth. In this case, we see that the penetration depth of the liquid PS front increases as annealing time increases, but the variation is clearly not linear. For example, at 160 °C the front position, initially at 190 μm, changes to 170 μm after 0.75 h, to 140 μm after 7 h, and then only reaches a value of 70 μm after 57 h. These data are not consistent with a Case-II regime, characterized by a linear kinetics of liquid penetration. Comparing Figs. 5A and 5B we see that the front penetration rate in the pure glassy layer increases markedly with temperature. It would be possible, for example, to analyze the temperature dependence of the advancing front rate in terms of activation energies and to evaluate whether the values obtained correspond to those characteristic of viscous flow, associated with Fickean diffusion, or, on the contrary, they can be compared with those characteristic of yielding of glassy polymers, associated with a mechanism of mechanically controlled penetration.

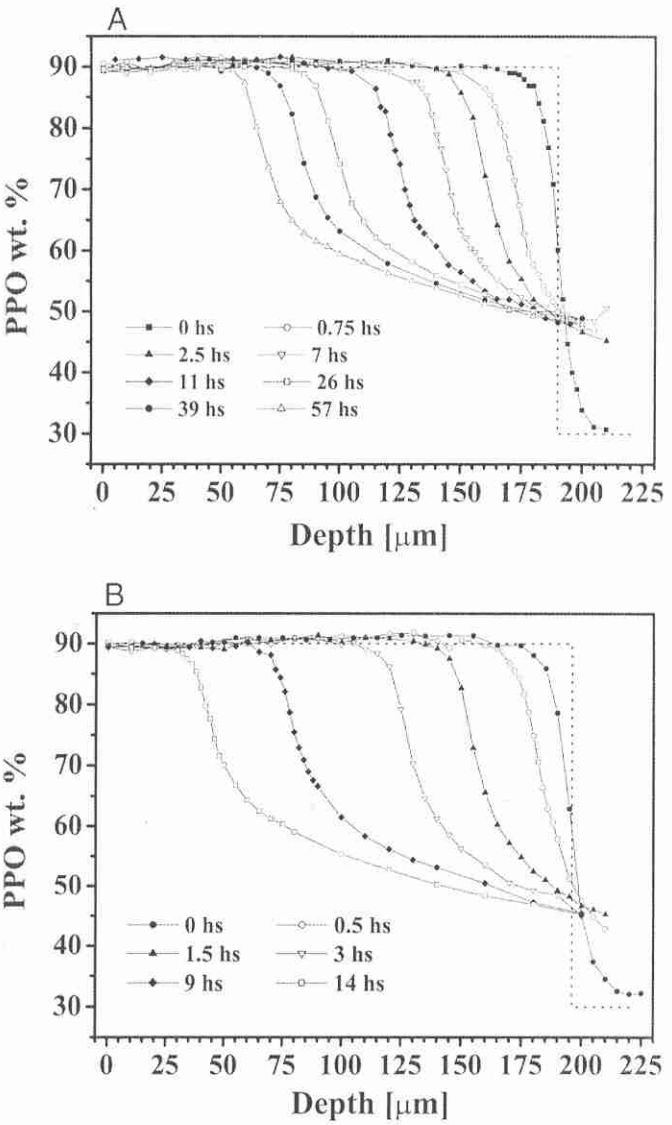

FIG. 5. Evolution of concentration profiles (PPO wt. % versus depth) at glassy-liquid interphases. Samples held at (**A**) 160 °C; and (**B**) 180 °C, for the times indicated in the plot.

The sharp fronts are followed at larger depths by a quite flat region, almost a plateau, clearly observed for those profiles corresponding to larger front advances or longer annealing times, but out of the 210 μm observational window for profiles obtained after short annealing times. Throughout this almost flat region, the PPO concentration is relatively uniform and increases over time, which indicates that PPO molecules are rapidly distributed in the liquid film. In fact, after a few hours of annealing, PPO molecules reach the outer surface of the PS-rich film. We could track the PPO distribution at the PS-rich layer surface by placing the composite specimen upside down on the microscope stage and using a "dry" objective to carry out a surface examination of the PS-rich layer (DPl method in Fig. 3). For example, for the sample annealed at 160 °C, we detected an increase in PPO concentration above 30 wt. %, the original concentration in the soft film, after 7 hours of annealing. This means that while the PS liquid front advanced only 60 μm in the glassy film direction (see the corresponding profile in Fig. 5A), PPO molecules traveled the whole thickness of the liquid film (about 1000 μm) up to reach its surface.

The relative rates of these processes (front advance versus distribution rate) reflect the huge changes in molecular mobilities that occur inside the liquid placed close to the glassy polymer layer, associated with the abrupt changes in T_g along the diffusion path. They are responsible for the asymmetry of the PS-liquid profiles, noticeably captured by the experimental technique. The direct observation of these profiles along with a rigorous analysis of the experimental evidence in terms of the issues discussed above should allow us to ascribe unambiguously the observed diffusion kinetics to a specific diffusion mechanism. This type of analysis will be carried out and reported on in forthcoming publications.

Correction of Depth Profiles by Spatial Deconvolution. Results from Fig. 5 show that, in the transition from the PS-rich liquid layer to the PPO-rich glassy layer, the PS fronts appear systematically rounded and preceded by a tail 10 to 15 μm in size, on the order of the depth resolution of the technique. It has been well established that the presence of concentration tails preceding the advance of the diffusion front is distinctive of certain non-Fickean diffusion mechanisms.[3,9] On the other hand, and due to the fact that diffusivities are the lowest at the diffusion front, a very sharp (almost vertical) transition

between layers should be expected for the case of Fickean diffusion.[13,16] Therefore, from a mechanistic point of view, to discern whether these tails are produced by genuine mass transport or are due to artificial broadening becomes very important. To address this point, we corrected the experimental profiles from instrumental broadening by deconvolution, using the generalized inversion method developed by our group. Full details of the numerical technique can be found in Ref. 27, and here we summarize its main characteristics. The approach is based on the Philips–Tilkonov regularization method, with the instrumental broadening function (IBF) as a spatially invariant convolution kernel. The regularization parameter (γ) is pondered locally along the interphase as a Gaussian function with standard deviation σ_γ. The Gaussian is centered in the point of maximum change of the composition profile, which is computed numerically. Regularization is applied in such a way that it is null at this point and then increases at both sides, reaching a maximum in those regions where the profile is known to be smooth.[27]

The correction scheme relies on the precise knowledge of the IBF. If refraction effects are effectively minimized, most parts of the broadening in depth-profiling experiments should only arise from a combination of diffraction/instrumental factors, which can be assumed invariant (or depth independent).[17,28] A good experiment to characterize IBF is the measure of the Raman step-response of a silicon wafer in the z direction, even though other approaches have recently been proposed.[26,28] As the laser beam does not penetrate significantly into silicon, the wafer surface behaves essentially like a layer of infinitesimal thickness, and the experiment provides a point-by-point measure of IBF. The Raman profile corresponding to this experiment was already shown in Fig. 1. Note that the depth resolution measured as the FWHM (~6 μm) is slightly larger than others reported in the literature (2–4 μm), which might be attributed to variations in transmission of the different objectives used, as we adapted to immersion optics an instrument originally designed to operate with dry objectives.

For deconvolution calculations, we used the silicon profile shown in Fig. 2 as IBF, with γ determined by the generalized cross-validation technique in the range 10^3–10^4. The value for σ_γ was 20.[27] Figure 6 shows interphase profiles after correction for the sample annealed at 180 °C. In Fig. 6A we compare raw and corrected PPO concentration profiles for one of the diffusion times (14 h) on a finer scale in order to facilitate visual comparison. Figure 6B shows the whole set of data using the same scale as in Fig. 5.

We see that deconvolution eliminates almost completely the tails observed at the left hand of the PS fronts in the raw profiles, making the fronts much sharper. The correction reveals that the transition from glassy to liquid occurs over a much narrower range of depths (less than 4 μm). The enhancement in depth resolution can be estimated by comparing the FWHM of the first-derivative curves corresponding to raw and deconvoluted data, as detailed elsewhere.[28] On average, FWHM decreases from 14 μm in the raw data to 4 μm after deconvolution, a value very close to that obtained by surface profiling of a sharp interface without diffusion, as shown in Fig. 4. This indicates that the glassy-to-liquid transition is indeed very sharp. At the same time, the spatial resolution attained after deconvolution is comparable to what one would obtain by physical sectioning and surface profiling, but keeping the flexibility and nondestructive nature

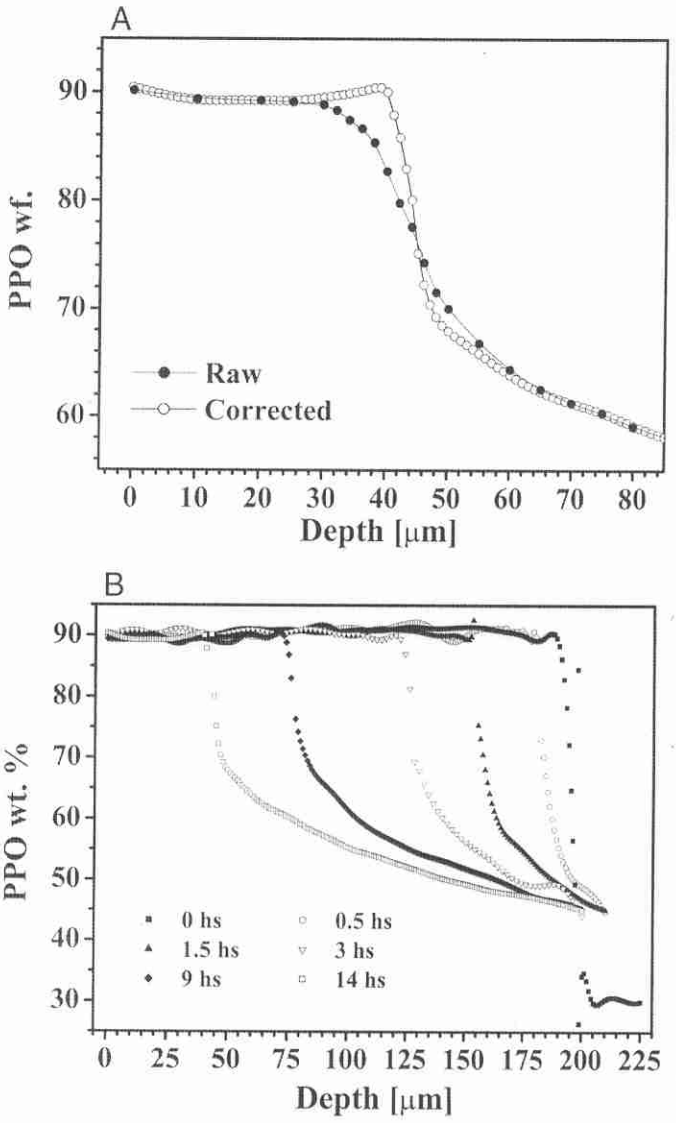

FIG. 6. Interphase concentration profiles corrected by regularized deconvolution for the sample annealed at 180 °C. (A) Comparison with uncorrected data. (B) Whole set of data. See text for parameters used in the deconvolution.

of optical sectioning. One of the benefits of the locally pondered regularization strategy is that spurious oscillations, typical of ill-conditioned problems, are absent, but at the same time the details of the abrupt transition at the interphase are well preserved. In this sense, the method appears to be more precise than others proposed in the literature for this case, see for example Figs. 8 and 11 in Ref. 28.

CONCLUSION

We described an integral approach to the study of interphase evolution in polymer films by CRM, which takes advantage of the noninvasive nature of depth profiling, the ability to perform point-by-point spatial measurements, and the improved depth resolution by means of the implementation of immersion optics. The use of an efficient deconvolution scheme based on locally pondered regularization additionally enhances spatial resolution, up to levels one would obtain with surface profiling, but without its inconvenient features. Overall, the experimental setup allows the acquisition of highly reproducible experimen-

tal data, with well-defined spatial resolution and no interference of the coupling oil with the process we want to study.

The liquid-glassy interphase studied here still offers many challenges and aspects to be understood in terms of the mechanisms that control interphase evolution. From this perspective, the experiment captures the most important features needed to discern the factors that control this process, an issue that will be addressed in future publications. In combination with the experimental setup described here and the improvements in depth resolution, confocal Raman microspectroscopy emerges as the best approach for the study of diffusion kinetics in this type of system.

ACKNOWLEDGMENTS

This work was funded by ANPCyT (PICT 12-14570) and by CYTED (project VIII.11). J.P. Tomba would like to thank Drs. M. Herguedas and L. Izaguirre for their valuable assistance during CRM measurements.

1. P. G. de Gennes, J. Chem. Phys. **55,** 572 (1971).
2. E. J. Kramer, P. F. Green, and C. J. Palmstrom, Polymer **25,** 473 (1984).
3. N. L. Thomas and A. H. Windle, Polymer **21,** 613 (1980).
4. M. Geoghegan, R. A. L. Jones, M. G. D. Van der Grinten, and A. S. Clough, Polymer **40,** 2323 (1999).
5. Q.-Y. Zhou, A. S. Argon, and R. E. Cohen, Polymer **42,** 613 (2001).
6. C. J. Lin, I. F. Tsai, C. M. Yang, M. S. Hsu, and Y. C. Ling, Macromolecules **36,** 2464 (2003).
7. J. P. Tomba, J. M. Carella, D. García, and J. M. Pastor, Macromolecules **38,** 4355 (2005).
8. R. J. Composto, E. J. Kramer, and D. M. White, Macromolecules **21,** 2580 (1988).
9. P. F. Nealey, R. E. Cohen, and A. S. Argon, Polymer **36,** 3687 (1995).
10. T. E. Shearmur, A. S. Clough, D. W. Drew, M. G. D. van der Grinten, and R. A. L. Jones, Macromolecules **29,** 7269 (1996).
11. P. F. Green and B. L. Doyle, Macromolecules **20,** 2471 (1987).
12. Y. Ma, J. P. S. Farinha, M. A. Winnik, P. V. Yaneff, and R. A. Ryntz, Macromolecules **37,** 6544 (2004).
13. E. A. Jordan, R. C. Ball, A. M. Donald, L. J. Fetters, R. A. L. Jones, and J. Klein, Macromolecules **21,** 235 (1988).
14. S. Hajatdoost, M. Olsthoorn, and J. Yarwood, Appl. Spectrosc. **51,** 1784 (1997).
15. J. Sacristán, C. Mijangos, H. Reinecke, S. Spells, and J. Yarwood, Macromolecules **33,** 6134 (2000).
16. J. P. Tomba, J. M. Carella, J. M. Pastor, and J. C. Merino, Polymer **43,** 6751 (2002).
17. N. Everall, Appl. Spectrosc. **54,** 1515 (2000).
18. N. Everall, Appl. Spectrosc. **54,** 773 (2000).
19. K. J. Baldwin and D. N. Batchelder, Appl. Spectrosc. **55,** 517 (2001).
20. J. L. Bruneel, J. C. Lassègues, and C. Sourisseau, J. Raman Spectrosc. **33,** 815 (2002).
21. C. Sourisseau and P. Maraval, Appl. Spectrosc. **57,** 1324 (2003).
22. J. P. Tomba, E. de la Puente, and J. M Pastor, J. Polym. Sci., Part B: Polym. Phys. **38,** 1013 (2000).
23. A. H. Kuptsov and G. N. Zhizhin, *Handbook of Fourier Transform Raman and Infrared Spectra of Polymers* (Elsevier, New York, 1998).
24. M. Prest and R. S. Porter, J. Polym. Sci., Part A: Polym. Chem. **10,** 1639 (1972).
25. J. Brandrup, E. H. Immergut, and E. A. Grulke, *Polymer Handbook* (John Wiley and Sons, New York, 1999).
26. J. Vyorykka, J. Halttunen, H. Iitti, J. Tenhunen, T. Vuorinen, and P. Stenius, Appl. Spectrosc. **56,** 776 (2002).
27. J. P. Tomba and G. Elicabe, Appl. Spectrosc. **57,** 920 (2003).
28. J. Vyorykka, J. Paaso, M. Tenhunen, H. Iitti, T. Vuorinen, and P. Stenius, Appl. Spectrosc. **57,** 1123 (2003).